

# Exploring patterns of demand in bike sharing systems via replicated point process models

Daniel Gervini and Manoj Khanal  
Department of Mathematical Sciences  
University of Wisconsin–Milwaukee

June 14, 2019

## Abstract

Understanding patterns of demand is fundamental for fleet management of bike sharing systems. In this paper we analyze data from the Divvy system of the city of Chicago. We show that the demand of bicycles can be modeled as a multivariate temporal point process, with each variable corresponding to a bike station in the network. The availability of daily replications of the process allows nonparametric estimation of the intensity functions, even for stations with low daily counts, and straightforward estimation of the correlations between stations. These correlations are then used for clustering, which reveal different patterns of demand.

*Key words:* Doubly-stochastic process; functional data analysis; latent-variable model; Poisson process; spatial process.

# 1 Introduction

Bike sharing systems are becoming increasingly common in large cities around the world (Shaheen et al., 2010). These systems provide short-term bicycle rental services at unattended stations throughout the cities. A user checks out a bicycle at a station near the origin of the journey and checks it back in at a station near the intended destination. For the system to run smoothly, it is necessary that both bicycles and empty slots be available at every station. If no bicycles are available at the intended origin of the trip, the user needs to start looking for alternative stations farther away, which may dissuade them from using the system altogether. A similar problem arises if there are no empty slots at the intended destination and the user needs to look for alternative stations to return the bike. Since bike flow from one station to another is rarely matched by a similar flow in the reverse direction, imbalances in the spatial distribution of bikes inevitably arise (Nair and Miller-Hooks, 2011). There are different strategies to manage this problem. For example, bikes are manually relocated by trucks as part of the day-to-day operation of the system. From a longer-term perspective, careful planning of the location of new stations is important. In order to make good short- and long-term decisions, understanding the spatiotemporal patterns of demand is fundamental.

In this paper we show that bike demand at each station can be modeled as a temporal point process, where bike checkout time is the random event of interest. Bike return can be modeled in a similar way. We will analyze data from the Divvy system in the city of Chicago, which is publicly available at the Chicago Data Portal website. Specifically, we will analyze bike trips that took place between April 1 and November 30 of 2016, since bike usage considerably decreases during the winter. There were a total of 3,068,211 bike trips and 458 active bike stations in that period. Demand varies a lot depending on the station location, from a lowest of 29 annual trips for station 386 in the South Side to a highest of 85,314 annual trips for station 35 in the Navy Pier. For stations with relatively large daily counts the distribution of bike demand on any given day can be estimated by kernel smoothing or similar density estimation methods (Silverman, 1986). But for stations with low daily counts this is not possible. In this paper we propose a new model that overcomes this deficiency by “borrowing” data from different days, similar to functional principal component models (Ramsay and Silverman, 2005), allowing estimation of daily distributions of

bike demand even for stations with low daily counts. We then use these estimators to study the spatial correlations between stations, and derive clusters that can be identified with different usage patterns.

To put the problem in context, we note that different aspects of bike sharing systems have been studied in the specialized literature (e.g. Borgnat et al., 2011; Vogel et al., 2011; Nair et al., 2013), but estimation and modeling of daily demand distribution at every station in the network has not yet been addressed, to the best of our knowledge. From a statistical methodology perspective, the study of replicated point processes is a novel field and the literature is so far limited to univariate processes (e.g. Wu et al., 2013; Li and Guan, 2014; Bouzas and Ruiz-Fuentes, 2015; Gervini, 2016), not multivariate processes as in this paper. Finally, we mention that clustering of spatial functional data has been addressed in the literature (e.g. Delicado et al., 2010; Romano et al., 2010; Secchi et al., 2013; Menafoglio and Secchi, 2017) but in the context of a single datum per site, which does not allow for direct estimation of spatial correlations and requires assumptions such as isotropy. In this paper, the availability of replications makes it possible to estimate spatial correlations directly, without the isotropy assumption, which, in fact, we show not to hold for the bike sharing network.

## 2 Modeling daily bike demand

Let  $X_{ij}$  be the set of checkout times for day  $i$  at bike station  $j$ . In our data set we have  $n = 244$  days and  $d = 458$  bike stations.  $X_{ij}$  is a finite but otherwise random set, so it is best modeled as a point process. For an overview of point processes, see Møller and Waagepetersen (2004, ch. 2), Streit (2010, ch. 2) or Baddeley (2007).

A temporal point process  $X$  is a random countable set in  $[0, \infty)$ . A process is locally finite if  $\#(X \cap B) < \infty$  with probability one for any bounded interval  $B$ , in which case we can define the count function  $N(B) = \#(X \cap B)$ . A Poisson process is a locally finite process for which there exists a nonnegative locally integrable function  $\lambda(t)$  such that (i)  $N(B)$  follows a Poisson distribution with rate  $\int_B \lambda(t) dt$  for any bounded  $B$ , and (ii) for disjoint sets  $B_1, \dots, B_k$  the random variables  $N(B_1), \dots, N(B_k)$  are independent. A consequence of (i) and (ii) is that the conditional distribution of the points in  $X \cap B$  given  $N(B) = m$  is the distribution of  $m$  independent and identically distributed observations with density  $\lambda(t) / \int_B \lambda$ .

The function  $\lambda$  is called the intensity function of the process.

In our application we have  $nd$  processes  $X_{ij}$  with  $i = 1, \dots, n$  and  $j = 1, \dots, d$ , each with a corresponding intensity function  $\lambda_{ij}$  on the interval  $[0, 24]$ . Since the  $\lambda_{ij}$ s are nonnegative, we assume for simplicity that they are positive everywhere (even if negligible at some points) and model the logarithms of the  $\lambda_{ij}$ s instead.

For each station  $j$  we can model the daily departure of the log  $\lambda_{ij}$ s from an annual mean function  $\mu_j(t)$  as an additive principal component model, similar to those used in functional data analysis (Ramsay and Silverman, 2005, ch. 8):

$$\log \lambda_{ij}(t) = \mu_j(t) + \sum_{k=1}^p u_{ikj} \phi_{kj}(t), \quad (1)$$

where  $\{\phi_{kj}\}_{k=1}^p$  are orthonormal functions,  $\bar{u}_{.kj} = 0$  for each  $k$ , and  $\overline{u_{.kj}u_{.k'j}} = 0$  for  $k \neq k'$ . The  $p$  terms are typically arranged in decreasing order of variances  $\overline{u_{.kj}^2}$  for  $k = 1, \dots, p$ . For simplicity we use the same  $p$  for all stations, although  $p$  could vary with  $j$ . This additive model for the log  $\lambda_{ij}$ s turns into a multiplicative model for the  $\lambda_{ij}$ s:

$$\lambda_{ij}(t) = \lambda_{0j}(t) \prod_{k=1}^p \psi_{kj}(t)^{u_{ikj}}, \quad (2)$$

where  $\lambda_{0j}(t) = \exp \mu_j(t)$  and  $\psi_{kj}(t) = \exp \phi_{kj}(t)$ . We will refer to  $\lambda_{0j}(t)$  as the baseline intensity function for station  $j$ .

Since the  $\lambda_{ij}$ s are not directly observable, the mean  $\mu_j(t)$  and the components  $\phi_{kj}(t)$  must be estimated from the  $X_{ij}$ s. To facilitate this we use spline models (De Boor, 1978) for these functional parameters:

$$\mu_j(t) = \sum_{l=1}^q c_{l0j} \gamma_l(t), \quad \phi_{kj}(t) = \sum_{l=1}^q c_{lkj} \gamma_l(t),$$

where  $\{\gamma_l\}_{l=1}^q$  is a spline basis. We use B-splines in this paper, but other bases can be used, even non-spline bases such as the Fourier basis. Modeling  $\mu_j$  and the  $\phi_{kj}$ s as spline functions turns the functional estimation problem into a simpler multivariate problem of estimating the basis coefficients  $\mathbf{c}_{kj} = (c_{1kj}, \dots, c_{qkj})^T$ . It also simplifies the introduction of periodicity constraints: the intensity functions should satisfy  $\lambda_{ij}(0) = \lambda_{ij}(24)$ , and this can be enforced by the simple linear constraints  $\mathbf{c}_{kj}^T \boldsymbol{\gamma}(0) = \mathbf{c}_{kj}^T \boldsymbol{\gamma}(24)$ , where  $\boldsymbol{\gamma}(t) = (\gamma_1(t), \dots, \gamma_q(t))^T$ . Similarly, the orthonormality of the  $\phi_{kj}$ s

is enforced by the constraints  $\mathbf{c}_{k'j}^T \mathbf{J} \mathbf{c}_{kj} = \delta_{k,k'}$ , where  $\mathbf{J} = \int \boldsymbol{\gamma}(t) \boldsymbol{\gamma}(t)^T dt$  and  $\delta_{k,k'}$  is Kronecker's delta.

Fitting model (1), then, involves estimation of the parameters  $\mathbf{c}_{kj}$ s and the component scores  $u_{ikj}$ . We do this by maximum likelihood, using the Poisson model as working model. In view of the above-mentioned properties of the Poisson process, the density function of  $X_{ij} = \{t_{ij1}, \dots, t_{ijm_{ij}}\}$  is

$$f_{ij}(m_{ij}, t_{ij1}, \dots, t_{ijm_{ij}}) = \exp\left(-\int \lambda_{ij}\right) \prod_{l=1}^{m_{ij}} \lambda_{ij}(t_{ijl})$$

(if  $m_{ij} = 0$ , i.e.  $X_{ij} = \emptyset$ , then  $f_{ij}(0, \emptyset) = \exp(-\int \lambda_{ij})$ .) Then, for each station  $j$ , we find the estimators  $\hat{\mathbf{c}}_{kj}$ s and  $\hat{u}_{ikj}$ s by maximizing the log-likelihood function

$$\begin{aligned} \ell &= \sum_{i=1}^n \log f_{ij}(m_{ij}, t_{ij1}, \dots, t_{ijm_{ij}}) \\ &= -\sum_{i=1}^n \int \lambda_{ij} + \sum_{i=1}^n \sum_{l=1}^{m_{ij}} \log \lambda_{ij}(t_{ijl}), \end{aligned} \quad (3)$$

subject to the constraints mentioned above.

The mean  $\mu_j$  and the components  $\phi_{kj}$  are common to all days  $i$  for each given station  $j$ , so they are estimated from the combined observations of all  $n$  days. The component scores  $u_{ikj}$  are specific to each day, but they are only  $p$ , and  $p$  is typically small. So it is usually not problematic to estimate the  $u_{ikj}$ s, even for small  $m_{ij}$ s.

Once the mean  $\mu_j$ , the components  $\phi_{kj}$ s and the scores  $u_{ikj}$ s have been estimated, the daily intensity functions can be estimated from model (1) as

$$\hat{\lambda}_{ij}(t) = \exp\left\{\hat{\mu}_j(t) + \sum_{k=1}^p \hat{u}_{ikj} \hat{\phi}_{kj}(t)\right\}. \quad (4)$$

These can be subsequently used for spatial inference regarding, for instance, cross-correlations among bike stations, as we will see in Section 3.

Our preliminary simulation studies showed that, although the estimators of the functional parameters  $\mu_j$  and  $\phi_{kj}$ s were consistent, the variance of the  $\hat{u}_{ikj}$ s tended to be larger than the variance of the true  $u_{ikj}$ . To ameliorate this problem we re-scale the  $\hat{u}_{ikj}$ s as follows: let  $\tilde{u}_{ikj} = \tau_j \hat{u}_{ikj}$ , and estimate  $\tau_j$  by maximum likelihood based

on the  $m_{ij}$ s; that is,  $\hat{\tau}_j$  maximizes

$$\begin{aligned}\tilde{\ell}_j &= \sum_{i=1}^n \log f_{ij}(m_{ij}) \\ &= - \sum_{i=1}^n I_{ij}(\tau) + \sum_{i=1}^n m_{ij} \log I_{ij}(\tau),\end{aligned}$$

where  $I_{ij}(\tau) = \int \hat{\lambda}_{ij}^{(\tau)}(t) dt$  and  $\hat{\lambda}_{ij}^{(\tau)}(t)$  is as in (4) with  $\hat{u}_{ikj}$  replaced by  $\tau \hat{u}_{ikj}$ .

Another refinement of the procedure, which improves the estimation of  $\mu_j$  and the  $\phi_{kj}$ s, is to add regularization terms to the log-likelihood function (3). The roughness of the function  $\mu_j$  can be measured by the functional norm of its second derivative,  $\int (\mu_j'')^2$ , and similarly with the  $\phi_{kj}$ s, so we obtain smoother estimators by maximizing the penalized log-likelihood function

$$P\ell = \ell - \xi_1 \int (\mu_j'')^2 - \xi_2 \sum_{k=1}^p \int (\phi_{kj}'')^2, \quad (5)$$

where  $\xi_1$  and  $\xi_2$  are non-negative tuning parameters that regulate the degree of smoothness of  $\mu_j$  and the  $\phi_{kj}$ s, respectively. These parameters can be chosen subjectively or by more objective (but more time-consuming) methods like cross-validation (Hastie et al., 2009, ch. 7). We found in our simulations that even a quick subjective choice of smoothing parameters offers considerable improvement over not regularizing the estimators.

### 3 Spatial correlations and clustering

In multivariate analysis, a measure of overall correlation between two random vectors  $\mathbf{U}$  and  $\mathbf{V}$  is the correlation coefficient  $\rho = \max_{\mathbf{a}, \mathbf{b}} \text{corr}(\mathbf{a}^T \mathbf{U}, \mathbf{b}^T \mathbf{V})$ , the largest possible correlation between linear combinations of  $\mathbf{U}$  and  $\mathbf{V}$  (Izenman, 2008, ch. 7.3). This coefficient can be computed as follows: let  $\Sigma_{UU}$  be the covariance matrix of  $\mathbf{U}$ ,  $\Sigma_{VV}$  the covariance matrix of  $\mathbf{V}$ , and  $\Sigma_{UV}$  the cross-covariance matrix of  $\mathbf{U}$  and  $\mathbf{V}$ ; then  $\rho^2$  is the largest eigenvalue of  $\Sigma_{UU}^{-1/2} \Sigma_{UV} \Sigma_{VV}^{-1} \Sigma_{VU} \Sigma_{UU}^{-1/2}$ , or equivalently, of  $\Sigma_{VV}^{-1/2} \Sigma_{VU} \Sigma_{UU}^{-1} \Sigma_{UV} \Sigma_{VV}^{-1/2}$ . The sample canonical correlation coefficient is obtained by substituting sample covariance matrices.

In functional data analysis, where  $U(t)$  and  $V(t)$  are square-integrable stochastic

processes, a functional version of the canonical correlation coefficient is used (Horváth and Kokoszka, 2012):  $\rho = \max_{\alpha, \beta} \text{corr}(\langle \alpha, U \rangle, \langle \beta, V \rangle)$ , where  $\alpha$  and  $\beta$  are square-integrable functions and  $\langle f, g \rangle = \int f(t)g(t)dt$ . As we show in the Appendix, the computation of  $\rho$  is analogous to the multivariate case, using the principal component scores of  $U$  and  $V$ .

In our application, we are interested in the correlation of bike demand at different stations  $j$  and  $j'$ , so we define

$$\hat{\rho}_{jj'} = \max_{\alpha, \beta} \text{corr}(\langle \alpha, \log \hat{\lambda}_{ij} \rangle, \langle \beta, \log \hat{\lambda}_{ij'} \rangle). \quad (6)$$

As shown in the Appendix,  $\hat{\rho}_{jj'}^2$  is the largest eigenvalue of  $\mathbf{S}_{jj}^{-1/2} \mathbf{S}_{jj'} \mathbf{S}_{j'j}^{-1} \mathbf{S}_{j'j} \mathbf{S}_{jj}^{-1/2}$ , where  $\mathbf{S}_{jj}$  is the sample covariance matrix of the estimated component scores  $\hat{\mathbf{u}}_{ij}$ s, where  $\hat{\mathbf{u}}_{ij} = (\hat{u}_{i1j}, \dots, \hat{u}_{ipj})^T$ , and  $\mathbf{S}_{jj'}$  is the sample cross-covariance matrix of the  $\hat{\mathbf{u}}_{ij}$ s and the  $\hat{\mathbf{u}}_{ij'}$ s.

The fact that there are  $n$  replications of the process for each site  $j$ , and consequently  $n$   $\hat{\mathbf{u}}_{ij}$ s, allows straightforward estimation of  $\hat{\rho}_{jj'}$ . In contrast, applications of spatial functional data analysis where only one observation per site is available require more complicated estimation of spatial correlations, usually under assumptions such as isotropy (e.g. Delicado et al., 2010; Menafoglio and Secchi, 2017). Here we do not need to make assumptions about the spatial correlation structure of the process and in fact we will see in Section 5 that isotropy does not hold for our data.

Once the correlations  $\hat{\rho}_{jj'}$  have been computed for all possible pairs  $(j, j')$ , we can use them, for instance, to discover clusters in the data. Clusters of stations with large  $\hat{\rho}_{jj'}$ s within clusters and low  $\hat{\rho}_{jj'}$ s between clusters would indicate that the network can be partitioned by patterns of usage (e.g. commute versus leisure). Such clusters can be obtained by applying standard agglomerative techniques (Izenman 2008, ch. 12.3) to distances defined by  $d_{jj'} = 1 - \hat{\rho}_{jj'}$ . For our application we found that complete linkage generally produces better results than single or average linkage.

When  $d$  is large there are many pairs  $(j, j')$  ( $d(d-1)/2 = 104,196$  in our application) so it is useful to trim non-significant  $\hat{\rho}_{jj'}$ s before clustering. A test for  $H_{0,jj'} : \rho_{jj'} = 0$  is the following (Seber 2004, ch. 5.7.3): let  $\{r_k^2\}$  be the  $p$  eigenvalues of  $\mathbf{S}_{jj}^{-1/2} \mathbf{S}_{jj'} \mathbf{S}_{j'j}^{-1} \mathbf{S}_{j'j} \mathbf{S}_{jj}^{-1/2}$  and  $\ell = \prod_{k=1}^p (1 - r_k^2)$ ; then  $Q_{jj'} = -(n-p) \log \ell$  is asymptotically  $\chi_\nu^2$  with  $\nu = p^2$  under the null hypothesis. We use Benjamini and Hochberg (1995) procedure to control the simultaneous type I error: let  $P_{jj'} =$



$P(\chi_{p^2}^2 > Q_{jj'})$  be the  $p$ -value for  $H_{0,jj'}$ , and  $\{P_{(k)}\}$  the set of these  $p$ -values sorted in increasing order, then the correlations considered significant are those for which  $P_{(k)} \leq \alpha k / \{d(d-1)/2\}$ , where  $\alpha$  is the desired simultaneous level. For the non-significant  $\hat{\rho}_{jj'}$ s we set  $\hat{\rho}_{jj'} = 0$ .

## 4 Simulations

In this section we study by simulation the consistency of the estimators proposed in Section 2. We simulated data from model (1) for a single location ( $d = 1$ ), since estimation is done separately in each location. We considered three distributional situations that will arise in the Divvy data analysis of Section 5: component scores that (i) are independent and identically distributed, (ii) follow a trend, and (iii) are autocorrelated. We also studied the effect of the expected number of observations per replication, the baseline rate  $\int \lambda_0(t)dt$ , which is determined by  $\mu$ .

To this end we considered model (1) with  $\mu(t) = \sin(\pi t) + c$ ,  $\phi_1(t) = \sqrt{2}\sin(\pi t)$  and  $\phi_2(t) = \sqrt{2}\sin(2\pi t)$ , for  $t \in [0, 1]$ . Since  $\int_0^1 \exp\{\sin(\pi t)\}dt = 1.98$ , we took  $c = \log 5$  and  $c = \log 15$ , which give baseline rates of approximately 10 and 30, respectively. The  $u_{ik}$ s were generated as follows:

1. Independent:  $u_{1k}, \dots, u_{nk}$  were independent  $N(0, \sigma_k^2)$  with  $\sigma_1 = .3\sqrt{.6}$  and  $\sigma_2 = .3\sqrt{.4}$ , respectively, so that the overall variance was .09, with the first component accounting for 60% of the variability. The  $u_{i1}$ s were independent of the  $u_{i2}$ s in this scenario and in the next two as well, since the scores of different components must be uncorrelated by assumption.
2. With quadratic trend: let  $s_i = -(i - n/2)^2$ , for  $i = 1, \dots, n$ . Then  $u_{i1} = \{(s_i - \bar{s})/\text{sd}(s_i)\}\sqrt{.75}\sigma_1 + z_i\sqrt{.25}\sigma_1$ , with  $z_i$ s independent and identically distributed  $N(0, 1)$ , and  $u_{i2}$ s independent and identically distributed  $N(0, \sigma_2^2)$ , with  $\sigma_1$  and  $\sigma_2$  as in Scenario 1. Note that the variance of  $u_{i1}$  is still  $\sigma_1^2$ , but now 75% of it comes from the quadratic trend.
3. Autocorrelated: the  $u_{i1}$ s followed the autoregressive model  $u_{i1} = z_i\sigma_e$  for  $i = 1$  and  $u_{i1} = \rho u_{i-1,1} + z_i\sigma_e$  for  $i = 2, \dots, n$ , with  $z_i$ s independent and identically distributed  $N(0, 1)$ ,  $\rho = .8$  and  $\sigma_e = \sigma_1\sqrt{1 - \rho^2}$ , so that the variance of the  $u_{i1}$ s was  $\sigma_1^2$ . The  $u_{i2}$ s were independent and identically distributed  $N(0, \sigma_2^2)$ , and we took  $\sigma_1$  and  $\sigma_2$  as in the previous scenarios.

$n$	Param	rate 10			rate 30		
		bias	std	rmse	bias	std	rmse
50	$\mu$	.45	1.33	1.40	.50	.88	1.01
	$\phi_1$	.39	.71	.81	.29	.62	.69
	$\phi_2$	.61	.83	1.04	.36	.69	.78
100	$\mu$	.53	.95	1.08	.55	.60	.82
	$\phi_1$	.30	.59	.66	.14	.44	.47
	$\phi_2$	.41	.72	.83	.22	.51	.56
200	$\mu$	.52	.64	.82	.53	.43	.68
	$\phi_1$	.20	.48	.52	.10	.30	.32
	$\phi_2$	.35	.62	.71	.17	.36	.40
400	$\mu$	.53	.45	.69	.53	.30	.61
	$\phi_1$	.21	.34	.40	.08	.21	.22
	$\phi_2$	.34	.57	.66	.16	.24	.29

Table 1: Simulation Results. Bias, standard deviation and root mean squared errors of parameter estimators for independent component scores (Scenario 1). Quantities for  $\mu$  were multiplied by 10.

To get an idea of the daily counts produced by these models, we generated a sample of size 100 for each baseline rate, and observed daily counts between 4 and 20 for baseline rate 10 and between 22 and 44 for baseline rate 30. Four sample sizes were considered in the study:  $n = 50, 100, 200$  and 400.

For estimation of the functional parameters we used a cubic B-spline basis with five equally spaced knots in  $(0, 1)$ . We computed estimators with and without regularization; for the former we used subjective but visually reasonable smoothing parameters  $\xi_1 = \xi_2 = 10^{-5}$ . We only report the regularized estimators here, since they produced overall better results.

Tables 1 to 3 report the results. For  $\mu$  we defined  $\text{bias} = \|E(\hat{\mu}) - \mu\|$ ,  $\text{std} = [E\{\|\hat{\mu} - E(\hat{\mu})\|^2\}]^{1/2}$  and  $\text{rmse} = \{E(\|\hat{\mu} - \mu\|^2)\}^{1/2}$ , where  $\|\cdot\|$  is the usual  $L^2[0, 1]$  norm. For the  $\phi_k$ s we could not use these quantities because of the sign indetermination (a priori, it is not possible to tell if  $\hat{\phi}_k$  is estimating  $\phi_k$  or  $-\phi_k$ ), so we considered the bivariate estimators  $\hat{\phi}_k(s)\hat{\phi}_k(t)$  of  $\phi_k(s)\phi_k(t)$  instead, which are sign-invariant, and defined bias, standard deviation and root mean squared errors as before, except that  $\|\cdot\|$  was the bivariate  $L^2$  norm on  $[0, 1] \times [0, 1]$ . The expectations were

$n$	Param	rate 10			rate 30		
		bias	std	rmse	bias	std	rmse
50	$\mu$	.46	1.29	1.37	.50	.82	.96
	$\phi_1$	.38	.70	.80	.25	.59	.64
	$\phi_2$	.60	.83	1.02	.35	.69	.78
100	$\mu$	.48	.91	1.02	.50	.59	.77
	$\phi_1$	.28	.60	.66	.17	.48	.51
	$\phi_2$	.45	.75	.87	.24	.54	.59
200	$\mu$	.50	.64	.82	.50	.40	.64
	$\phi_1$	.23	.46	.51	.10	.33	.35
	$\phi_2$	.34	.62	.71	.18	.38	.42
400	$\mu$	.49	.45	.66	.52	.30	.60
	$\phi_1$	.18	.34	.39	.08	.22	.23
	$\phi_2$	.34	.55	.65	.18	.31	.36

Table 2: Simulation Results. Bias, standard deviation and root mean squared errors of parameter estimators for component scores with a trend (Scenario 2). Quantities for  $\mu$  were multiplied by 10.

approximated by Monte Carlo based on 200 replications of each scenario.

Table 1 shows that, for independent and identically distributed component scores, the estimators behave as expected: estimation errors decrease as  $n$  increases for each baseline rate, and they are lower for the higher baseline rate. The bias of  $\hat{\mu}$  does not decrease with  $n$ , but this is due to the suboptimal choice of smoothing parameter (for the non-regularized estimators, not reported here, the bias of  $\hat{\mu}$  does go to zero as  $n$  increases).

Table 2 shows the results for Scenario 2, where the first component score follows a quadratic trend, and we see that they are almost identical to those in Table 1, so the estimators work equally well in both situations. Table 3 shows the results for Scenario 3, autoregressive component scores. The mean squared errors of  $\hat{\phi}_1$  and  $\hat{\phi}_2$  are somewhat larger than in the previous scenarios, but only by 20% at most, and they still decrease as  $n$  increases, so the estimators are also consistent in this scenario.

In addition to consistency of the parameter estimators, it is also important to study the consistency of the component score estimators  $\hat{u}_{iks}$ , since they are used for

$n$	Param	rate 10			rate 30		
		bias	std	rmse	bias	std	rmse
50	$\mu$	.46	1.56	1.63	.46	1.21	1.29
	$\phi_1$	.45	.75	.88	.45	.71	.84
	$\phi_2$	.60	.83	1.03	.50	.77	.92
100	$\mu$	.45	1.12	1.21	.43	.90	.99
	$\phi_1$	.29	.63	.69	.21	.52	.56
	$\phi_2$	.48	.77	.91	.25	.57	.62
200	$\mu$	.56	.83	1.00	.49	.64	.81
	$\phi_1$	.21	.50	.54	.12	.36	.38
	$\phi_2$	.36	.65	.74	.17	.40	.44
400	$\mu$	.47	.56	.74	.52	.45	.69
	$\phi_1$	.20	.34	.39	.09	.25	.26
	$\phi_2$	.35	.54	.64	.18	.30	.35

Table 3: Simulation Results. Bias, standard deviation and root mean squared errors of parameter estimators for autoregressive component scores (Scenario 3). Quantities for  $\mu$  were multiplied by 10.

$n$	Score	Independent				With trend				Autoregressive			
		rate 10		rate 30		rate 10		rate 30		rate 10		rate 30	
		eae	eac	eae	eac	eae	eac	eae	eac	eae	eac	eae	eac
50	pc 1	.28	.51	.18	.73	.28	.52	.17	.75	.29	.47	.20	.63
	pc 2	.26	.33	.17	.59	.26	.34	.17	.60	.26	.34	.19	.51
100	pc 1	.26	.54	.15	.77	.26	.54	.16	.77	.26	.52	.17	.73
	pc 2	.24	.40	.15	.67	.24	.39	.15	.65	.25	.37	.16	.63
200	pc 1	.24	.56	.14	.79	.24	.57	.14	.79	.24	.54	.15	.77
	pc 2	.23	.43	.14	.69	.23	.42	.14	.68	.23	.42	.14	.68
400	pc 1	.23	.58	.13	.80	.23	.57	.13	.80	.23	.57	.14	.79
	pc 2	.22	.43	.13	.70	.22	.43	.13	.68	.22	.43	.13	.69

Table 4: Simulation Results. Expected average error and expected absolute correlation of component score estimators under the three scenarios of Tables 1–3.

inference (like clustering, in this paper). The distance between the  $\hat{u}_{ik}$ s and the true  $u_{ik}$ s cannot be measured directly due, again, to the sign indeterminacy, so we use the estimation error of the variations  $v_{ik}(t) = u_{ik}\phi_k(t)$  instead. We define the expected average error  $eae = E(\sum_{i=1}^n \|\hat{v}_{ik} - v_{ik}\|/n)$ , where  $\|\cdot\|$  is the  $L^2[0,1]$  norm. We also measure the association between the  $\hat{u}_{ik}$ s and the  $u_{ik}$ s by the expected absolute correlation,  $eac = E\{|\text{corr}(\hat{u}_{ik}, u_{ik})|\}$ , which is sign-invariant.

Table 4 shows the results. Again we see consistency, that is, an improvement in estimation as  $n$  and/or the baseline rate increase. The baseline rate has a big impact on the performance of the  $\hat{u}_{ik}$ s, as expected, since the  $\hat{u}_{ik}$ s only use the  $m_i$  observations for each replication and cannot combine data across replications like  $\hat{\mu}$  and the  $\hat{\phi}_k$ s do. Regarding the three distributional scenarios, we see that there is almost no difference between the independent identically distributed case and the model with quadratic trend; the autoregressive model does show somewhat higher errors and lower correlations than the other two, especially for  $n = 50$ , but the difference tends to vanish as  $n$  increases. So we can conclude that the component score estimators are consistent under the three scenarios.

Figure 1: Baseline intensity function of daily bike demand for Divvy station 166, located at the intersection of Wrightwood and Ashland avenues.

## 5 Application: Chicago’s Divvy bike sharing system

As mentioned in the Introduction, we will analyze in this section the checkout times of bike trips that took place between April 1 and November 31 of 2016 in Chicago’s Divvy system. First, we fitted model (1) for the 458 bike stations that were active during this period. As spline basis for the functional parameters we used cubic B-splines with ten equally spaced knots in  $(0, 24)$ . We fitted models with  $p = 6$  components, which are sufficient to capture the more important modes of variability and can be estimated without inconvenient for most stations; only for station 386, the station with the lowest annual count, the model could not be fitted due to insufficient data.

It is clearly infeasible to visually inspect the results for all stations, but as an illustration we will analyze in more detail the results obtained for station 166, which is the station with median annual count. The estimated baseline intensity function  $\hat{\lambda}_{0,166}$  is shown in Figure 1. We see that  $\hat{\lambda}_{0,166}$  has three peaks: the first and largest one occurs at 7:30am, the second and smallest one at 1pm, and the third one at 5:30pm. The integral of  $\hat{\lambda}_{0,166}$  over  $[0, 24]$  is 17.66, very close to the mean daily count of 17.64, as expected.

Figure 2: First multiplicative component of daily bike demand for Divvy station 166. (a) Baseline (solid line) and baseline multiplied by a positive (dotted line) and negative (dashed line) exponent of the component. (b) Daily component scores as a time series.

To interpret the components  $\hat{\psi}_{k,j}$  it is instructive to plot the baseline function  $\hat{\lambda}_{0j}$  alongside  $\hat{\lambda}_{0j}^+ = \hat{\lambda}_{0j}\hat{\psi}_{kj}^c$  and  $\hat{\lambda}_{0j}^- = \hat{\lambda}_{0j}\hat{\psi}_{kj}^{-c}$ , for some positive constant  $c$  chosen for convenient visualization (here we take it as twice the standard deviation of the corresponding  $\hat{u}_{ikj}$ s). For the first component, this is shown in Figure 2(a). In Figure 2(b) we plotted the corresponding component scores  $\hat{u}_{i,1,166}$  as a time series on the index  $i$ . Figure 2(a) shows that a negative score corresponds to a sharpening of the morning peak and a positive score corresponds to a flattening of this peak. This corresponds to weekday versus weekend patterns of demand, respectively, as corroborated by Figure 2(b), which shows a steady weekly periodicity (the autocorrelation at lag 7 is .68), with peaks occurring almost always on Sundays and troughs mostly on Thursdays or Wednesdays. In Figure 3 we show the 244 estimated daily intensity functions, separating weekdays (Figure 3(a)) from weekends (Figure 3(b)); the absence of the morning peaks in Figure 3(b) is clear.

The second component (Figure 4(a)) explains overall count variation. Overall bike usage is strongly seasonal, as shown in Figure 4(b), with demand increasing from early Spring to Summer (the maximum occurs in June) and decreasing thereafter. The rest of the components explain finer-detailed aspects of bike demand variation.

After fitting model (2) for all bike stations, we computed the canonical correla-

Figure 3: Daily intensity functions of bike demand for Divvy station 166, (a) weekdays, (b) weekends.

Figure 4: Second multiplicative component of daily bike demand for Divvy station 166. (a) Baseline (solid line) and baseline multiplied by a positive (dotted line) and negative (dashed line) exponent of the component. (b) Daily component scores as a time series.



Figure 5: Dendrogram of complete-linkage clustering of bike stations in the Divvy system.

tions (6) for all pairs. The largest one turned out to be .98 and the smallest one .17. The largest correlation corresponds to bike stations 75 and 91, located at the main entrances of Union and Ogilvy train stations, respectively. Although these bike stations are relatively close to each other (four city blocks, or  $4.97 \times 10^{-3}$  in Euclidean distance), they are not the closest. For example, station 192 at the back entrance of Union Station also has correlation .98 with station 75, but station 73 is a distance  $2.63 \times 10^{-3}$  (two city blocks) from station 75 and their correlation is .90, and station 169 is a distance  $4.34 \times 10^{-3}$  from station 75 (as far as Ogilvy is, but in the opposite direction and not close to any train station) and their correlation is only .72. Therefore, it is clear that correlations are not functions of distance alone but also of type of usage; the process is not isotropic.

Then it is instructive to apply clustering methods to the correlations and try to associate the clusters with different patterns of usage. The clustering procedure of Section 3 gives the dendrogram shown in Figure 5. The vertical axis of the dendrogram indicates the distance of the objects being connected. Three big clusters are discernible in Figure 5, with a maximum distance of about .70, so the correlations of bike stations within the clusters are at least .30. These clusters include 136, 127 and 77 bike stations respectively, so they account for 340 of the 458 bike stations in the system.

The locations of stations in each cluster are shown in Figure 6. We also show the

Figure 6: Clusters of bike stations in the Divvy system. (a) Largest cluster, 136 stations; (b) second largest cluster, 127 stations, (c) third largest cluster, 77 stations.

Figure 7: Baseline density functions for the three clusters of bike stations in Figure 6.

baseline density functions for each station,  $\tilde{\lambda}_{0j} = \lambda_{0j} / \int \lambda_{0j}$ , in Figure 7. Although we are clustering by correlation and not by distance between baselines (which could be done), the baseline densities help interpret the type of usage given to the stations in each cluster. We see in Figure 7(a) that most densities in this cluster show a typical weekday usage pattern (compare with Figure 3(a)), and Figure 6(a) shows that most stations in downtown Chicago, and specifically in “the Loop”, belong to this cluster, so Cluster 1 consists of bike stations that are mostly used for commute. On the other hand, the densities in Figure 7(b) resemble a weekend usage pattern (compare with Figure 3(b)), and Figure 6(b) shows that most stations along the lake shore are in this cluster, so Cluster 2 consists of stations that are mostly used for leisure. The third cluster is somewhere in between.

## Acknowledgement

This research was partly supported by US National Science Foundation grant DMS 1505780.

## 6 Appendix

### 6.1 Computation of functional canonical correlations

Let  $U$  and  $V$  be two stochastic processes admitting finite expansions  $U(t) = \mu_U(t) + \sum_{k=1}^p u_k \phi_k(t)$  and  $V(t) = \mu_V(t) + \sum_{k=1}^q v_k \psi_k(t)$ , where the  $\phi_k$ s and the  $\psi_k$ s are orthonormal. The canonical correlation coefficient is  $\rho = \max_{\alpha, \beta} \text{corr}(\langle \alpha, U \rangle, \langle \beta, V \rangle)$ , where  $\alpha$  and  $\beta$  are arbitrary square-integrable functions. Any  $\alpha$  and  $\beta$  can be decomposed as  $\alpha(t) = \sum_{k=1}^p a_k \phi_k(t) + \eta(t)$  with  $\eta$  orthogonal to the  $\phi_k$ s and  $\beta(t) = \sum_{k=1}^q b_k \psi_k(t) + \xi(t)$  with  $\xi$  orthogonal to the  $\psi_k$ s. Then  $\langle \alpha, U - \mu_U \rangle = \sum_{k=1}^p a_k u_k$  and  $\langle \beta, V - \mu_V \rangle = \sum_{k=1}^q b_k v_k$ . Let  $\mathbf{a} = (a_1, \dots, a_p)$ ,  $\mathbf{U} = (U_1, \dots, U_p)$ ,  $\mathbf{b} = (b_1, \dots, b_q)$  and  $\mathbf{V} = (V_1, \dots, V_q)$ ; then  $\langle \alpha, U - \mu_U \rangle = \mathbf{a}^T \mathbf{U}$  and  $\langle \beta, V - \mu_V \rangle = \mathbf{b}^T \mathbf{V}$ . Since  $\text{corr}(\langle \alpha, U \rangle, \langle \beta, V \rangle) = \text{corr}(\langle \alpha, U - \mu_U \rangle, \langle \beta, V - \mu_V \rangle)$ , then  $\rho = \max_{\mathbf{a}, \mathbf{b}} \text{corr}(\mathbf{a}^T \mathbf{U}, \mathbf{b}^T \mathbf{V})$ , which is the standard multivariate canonical correlation coefficient for  $\mathbf{U}$  and  $\mathbf{V}$ . In particular, if  $U(t) = \log \lambda_j(t)$  and  $V(t) = \log \lambda_{j'}(t)$ , from model (1) we have that  $\mathbf{U}$  are the component scores for site  $j$  and  $\mathbf{V}$  are the component scores for site  $j'$ .

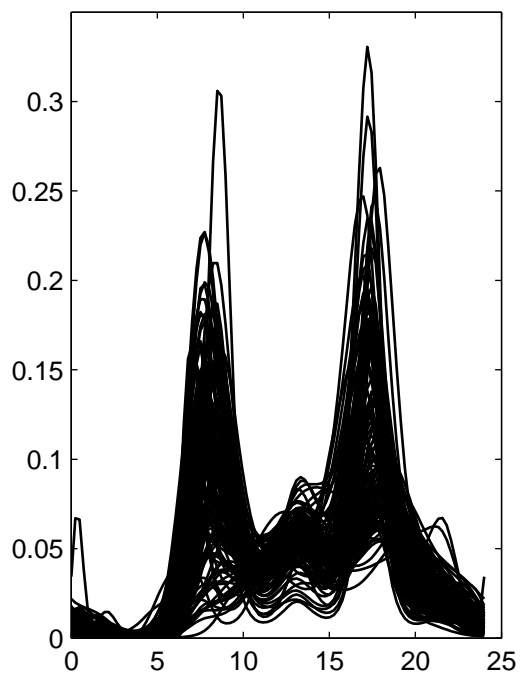
## References

- Baddeley, A. (2007). Spatial point processes and their applications. In *Stochastic Geometry*, Lecture Notes in Mathematics 1892, pp. 1–75. Springer, New York.
- Benjamini, Y., and Hochberg, Y. (1995). Controlling the false discovery rate: A practical and powerful approach to multiple testing. *Journal of the Royal Statistical Society Series B* **57** 289–300.
- Borgnat, P., Robardet, C., Rouquier, J., Abry, P., Flandrin, P., and Fleury, E. (2011). Shared bicycles in a city: A signal processing and data analysis perspective. *Advances in Complex Systems* **14** 1–24.
- Bouzas, P.R., and Ruiz-Fuentes, N. (2015). A review on functional data analysis for Cox processes. *Boletín de Estadística e Investigación Operativa* **31** 215–230.
- De Boor, C. (1978). *A Practical Guide to Splines*. Springer, New York.
- Delicado, P., Giraldo, R., Comas, C., and Mateu, J. (2010). Statistics for spatial functional data: Some recent contributions. *Environmetrics* **21** 224–239.
- Gervini, D. (2016). Independent component models for replicated point processes. *Spatial Statistics* **18** 474–488.
- Hastie, T., Tibshirani, R., and Friedman, J. (2009). *The Elements of Statistical Learning. Data Mining, Inference, and Prediction. Second Edition*. Springer, New York.
- Horváth, L., and Kokoszka, P. (2012). *Inference for Functional Data with Applications*. Springer, New York.
- Izenman, A.J. (2008). *Modern Multivariate Statistical Techniques. Regression, Classification and Manifold Learning*. Springer, New York.
- Li, Y., and Guan, Y. (2014). Functional principal component analysis of spatiotemporal point processes with applications in disease surveillance. *Journal of the American Statistical Association* **109** 1205–1215.

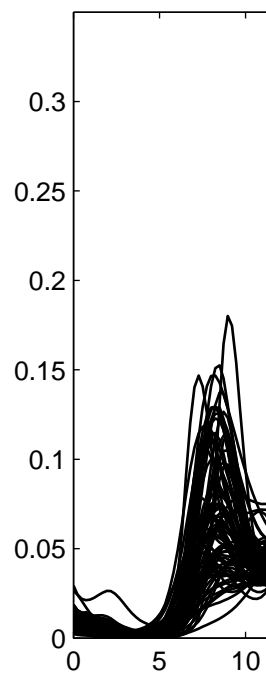
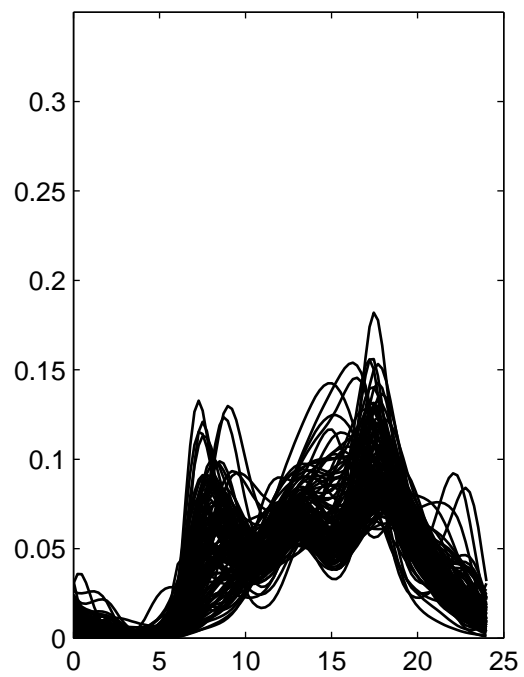
- Menafoglio, A., and Secchi, P. (2017). Statistical analysis of complex and spatially dependent data: A review of object oriented spatial statistics. *European Journal of Operational Research* **258** 401–410.
- Møller, J., and Waagepetersen, R.P. (2004). *Statistical Inference and Simulation for Spatial Point Processes*. Chapman and Hall/CRC, Boca Raton.
- Nair, R., and Miller-Hooks, E. (2011). Fleet management for vehicle sharing operations. *Transportation Science* **45** 524–540.
- Nair, R., Miller-Hooks, E., Hampshire, R.C., and Bušić, A. (2013). Large-scale vehicle sharing systems: Analysis of Vélib’. *International Journal of Sustainable Transportation* **7** 85–106.
- Ramsay, J. O., and Silverman, B. W. (2005). *Functional Data Analysis. Second Edition*. Springer, New York.
- Romano, E., Balzanella, A., and Verde, R. (2010). Clustering spatio-functional data: A model based approach. In *Classification as a tool for research. Studies in Classification, Data Analysis, and Knowledge Organization*, pp. 167–175. Springer, Berlin, Heidelberg.
- Seber, G.A.F. (2004). *Multivariate Observations*. Wiley, New York.
- Secchi, P. , Vantini, S. , and Vitelli, V. (2013). Bagging Voronoi classifiers for clustering spatial functional data. *International Journal of Applied Earth Observation and Geoinformation* **22** 53–64.
- Shaheen, S., Guzman, S., and Zhang, H. (2010). Bike sharing in Europe, the Americas and Asia: Past, present and future. *Transportation Research Record: Journal of the Transportation Research Board* **2143** 159–167.
- Silverman, B.W. (1986). *Density Estimation for Statistics and Data Analysis*. Chapman and Hall/CRC, Boca Raton.
- Streit, R.L. (2010). *Poisson Point Processes: Imaging, Tracking, and Sensing*. Springer, New York.

- Vogel, P., Greiser, T., and Mattfeld, D.C. (2011). Understanding bike-sharing systems using data mining: exploring activity patterns. *Procedia Social and Behavioral Sciences* **20** 514–523.
- Wu, S., Müller, H.-G., and Zhang, Z. (2013). Functional data analysis for point processes with rare events. *Statistica Sinica* **23** 1–23.

(a)



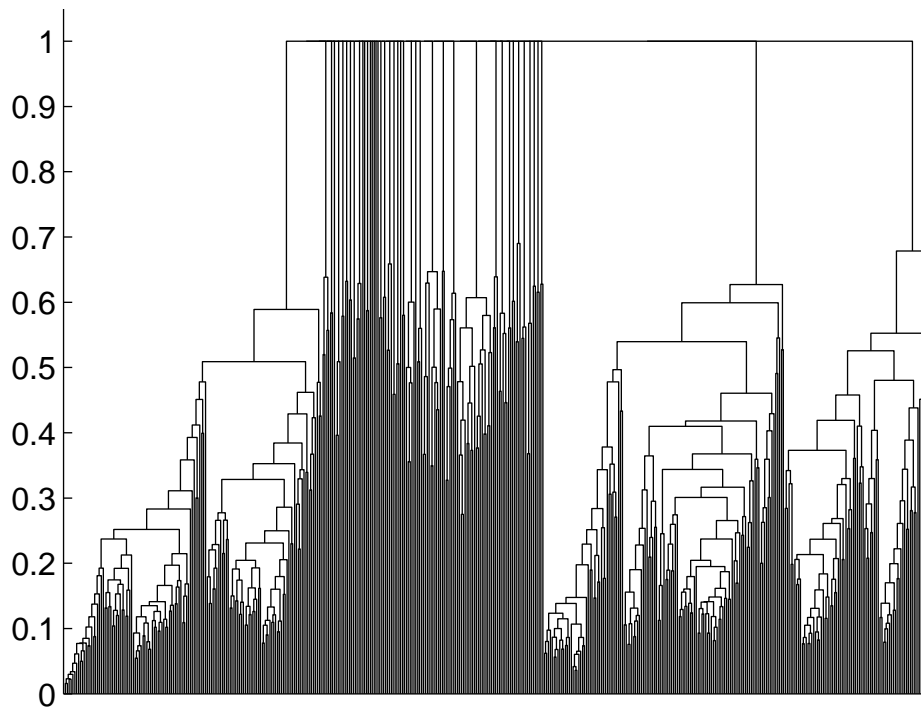
(b)

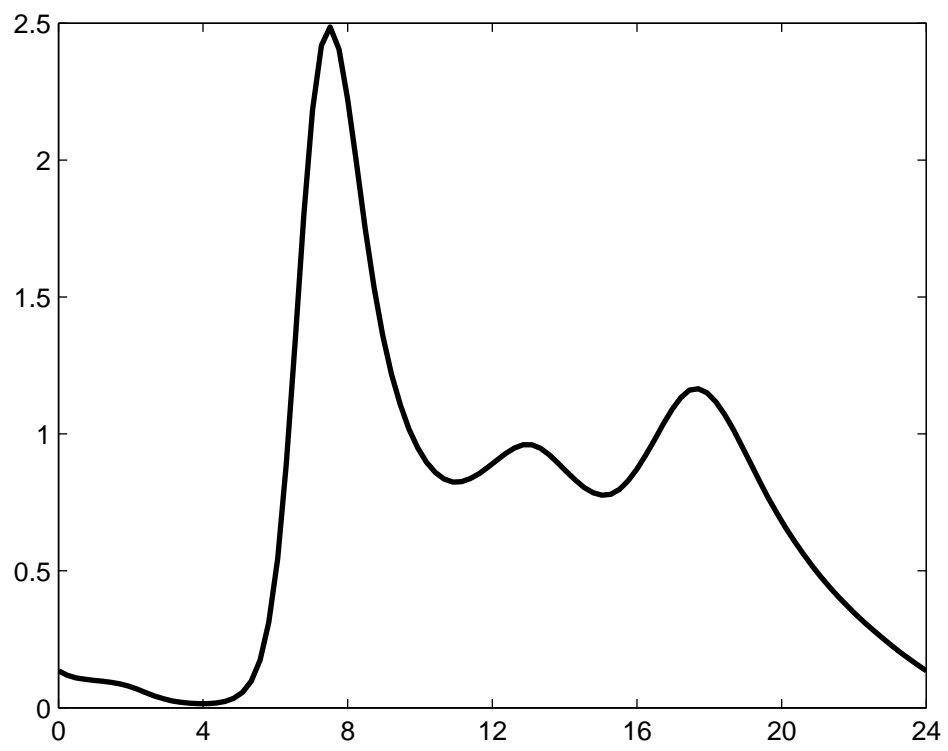


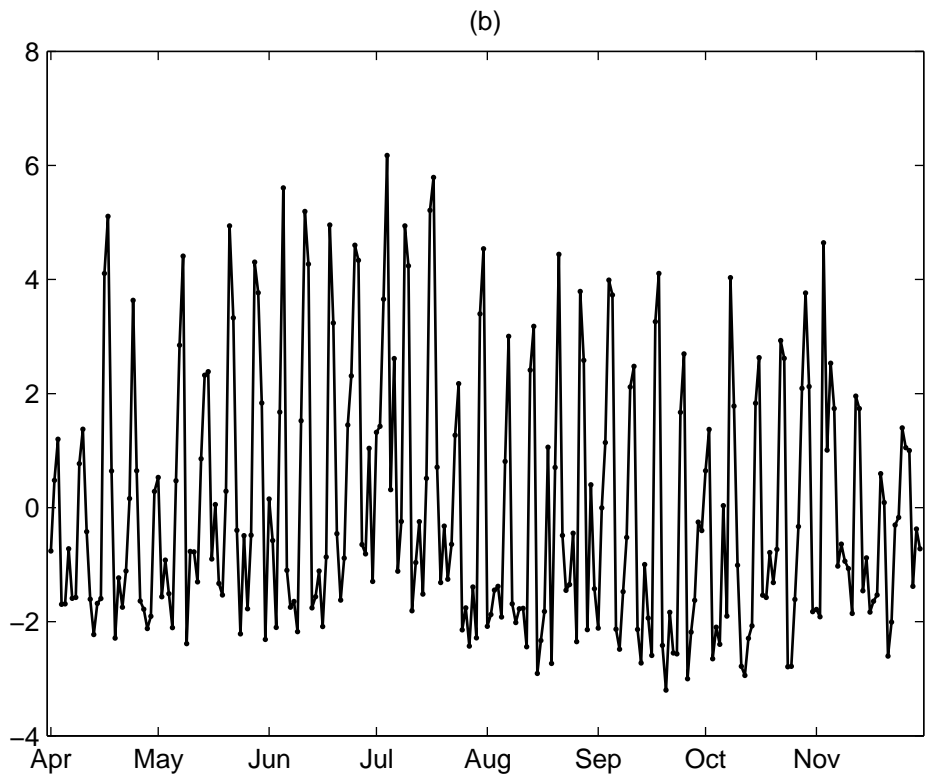
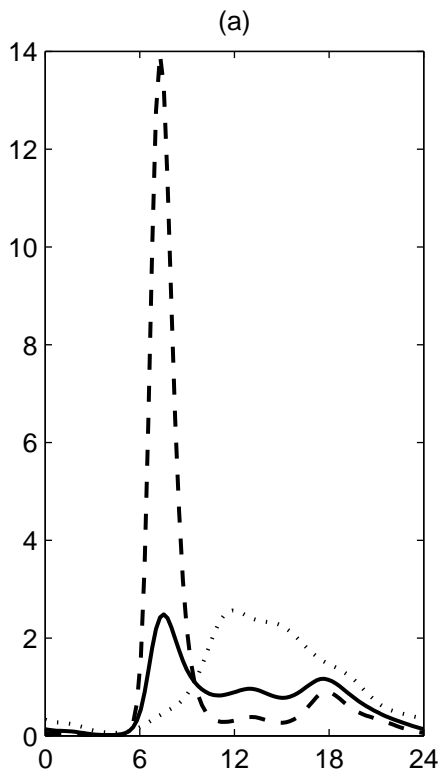
This figure "cluster\_points.jpg" is available in "jpg" format from:

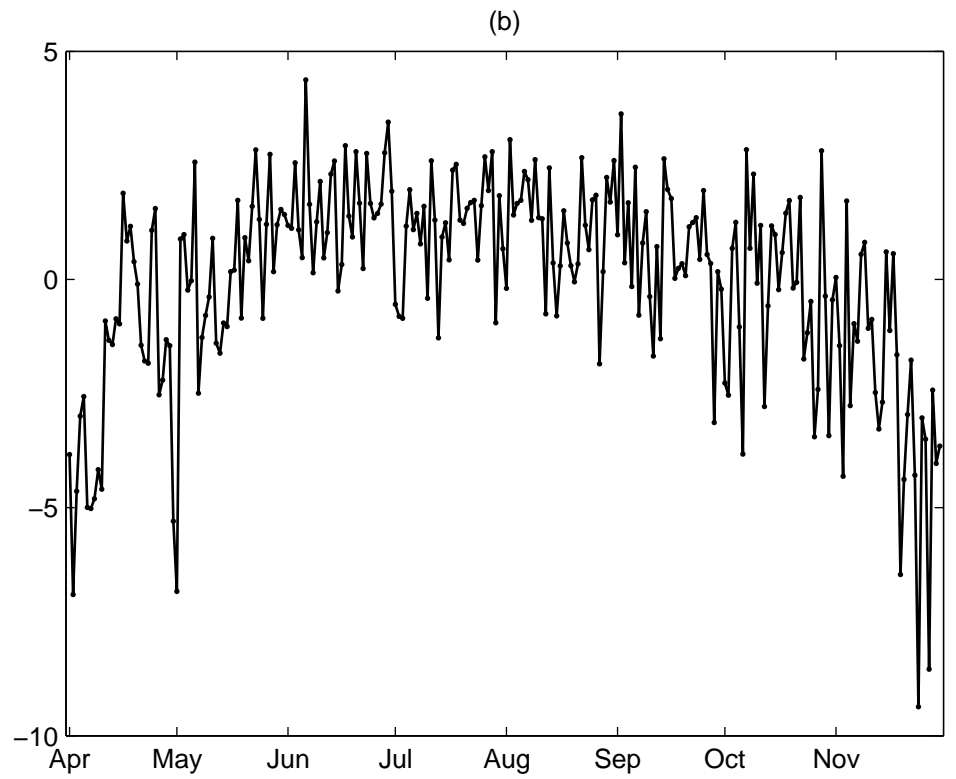
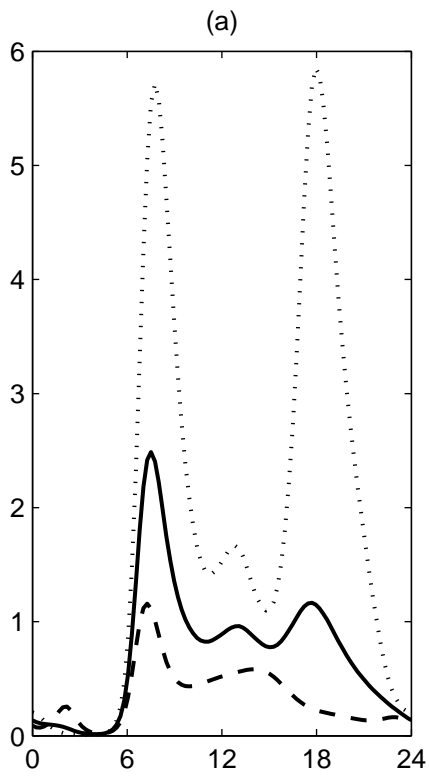
<http://arxiv.org/ps/1802.04755v1>



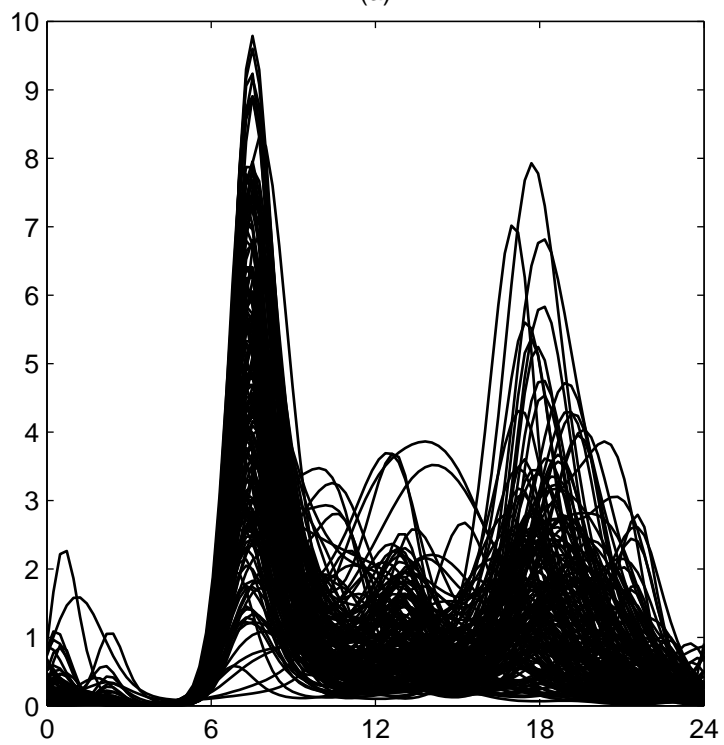








(a)



(b)

